Cavity piezomechanical strong coupling and frequency conversion on an aluminum nitride chip

Chang-Ling Zou,[1,2] Xu Han,[1] Liang Jiang,[2] and Hong X. Tang[1,2,*]
[1]*Department of Electrical Engineering, Yale University, New Haven, Connecticut 06511, USA*
[2]*Department of Applied Physics, Yale University, New Haven, Connecticut 06511, USA*
(Received 21 April 2016; published 6 July 2016)

Schemes to achieve strong coupling between mechanical modes of aluminum nitride microstructures and microwave cavity modes due to the piezoelectric effect are proposed. We show that the strong-coupling regime is feasible for an on-chip aluminum nitride device that is either enclosed by a three-dimensional microwave cavity or integrated with a superconducting coplanar resonator. Combining with optomechanics, the piezomechanical strong coupling permits coherent conversion between microwave and optical modes with high efficiency. Hence, the piezomechanical system will be an efficient transducer for applications in hybrid quantum systems.

DOI: 10.1103/PhysRevA.94.013812

I. INTRODUCTION

The efficient conversion between microwave and optical modes has attracted great attention recently [1–5]. The microwave-optical (M-O) interface between superconducting quantum circuits and optical photons is essential for quantum communications and distributed quantum computation networks [4,6,7]. A high-efficiency M-O converter will enable quantum state transfer and long-distance commutation between two microwave systems by optical fibers, without being impacted from microwave thermal noise at room temperature [8–10]. In addition, the M-O converter is also useful for single microwave photon level detectors [11–13]. Generally, the M-O conversion can be realized by either direct approaches or indirect approaches. The direct approaches harness the nonlinear optical effects in dielectrics, such as the electro-optic effect [14–16] and the magneto-optic effect [17]. The indirect approaches, on the other hand, exploit intermediate degrees of freedom to mediate the coupling between microwave and optical photons. For example, the reversible M-O conversion mediated by phonons has been proposed and demonstrated experimentally [18–20], where microwave and optical cavities are coupled to a common mechanical resonator. In addition, recently, the M-O conversion mediated by magnons has also been studied experimentally [21,22].

The coherent coupling between a microwave cavity and phonon modes due to piezoelectricity has been demonstrated [23,24], and the piezoelectric effect has also been utilized to actuate mechanical motion in optomechanical systems [24–29]. However, integrated systems with both piezoelectric coupling and optomechanical coupling for M-O conversion have neither been theoretically investigated nor experimentally demonstrated. In this paper, we propose a strongly coupled cavity piezo-optomechanical system for the M-O interface, where mechanical resonators on an aluminum nitride (AlN) chip are coupled with photonic and microwave cavities simultaneously. To distinguish from the electromechanics where the capacitive coupling between mechanical motion and microwave cavities would induce a frequency shift [18–20], we refer to the linear piezoelectric coupling as piezomechanics. Piezomechanical systems have several advantages: (i) The frequency of phonon can be near resonance with the microwave cavity, for example above 10 GHz, which relaxes the cryogenic temperature required to cool the system to the ground state. In contrast, in the flexible electromechanical system, the phonon frequency is usually orders smaller than that of the microwave photon to enable dispersive microwave photon-phonon coupling [19], and thus requires lower ambient temperature to suppress thermal phonon excitation. (ii) For near-resonant microwave and mechanical modes, both the microwave and the optical cavities are within the resolved-sideband regime, and thus the unwanted Stokes process (the parametric photon-phonon pair generation) is greatly suppressed. (iii) The microwave and mechanical modes are linearly coupled, hence an additional bias dc field or microwave field is not required. (iv) The systems proposed here are combined with integrated photonic chips [29], which are very robust and scalable.

The paper is organized as follows. In Sec. II, we study the basic features of cavity piezomechanics, develop the Hamiltonian description of the system, and discuss the possibility of ultrastrong piezomechanical coupling. Section III discusses the implementation in more realistic physical systems of AlN microstructures coupled to a three-dimensional (3D) microwave cavity or coupled to a quasi-two-dimensional coplanar cavity. With practical device parameters, it is estimated that piezomechanical coupling strength ranging from one to a few hundreds of MHz is feasible. In Sec. IV, the piezomechanical coupling is combined with the optomechanics, through which coherent M-O conversion is studied with optimized system parameters. High conversion efficiency ($\sim 90\%$) can be achieved, mainly limited by the intrinsic optical loss of the material. Section V summarizes the main results of this paper.

II. PIEZOMECHANICAL COUPLING

In general, the internal energy of a piezomechanical system is [30,31]

$$U = \frac{1}{2}\int dv(\mathbf{T}\cdot\mathbf{S} + \mathbf{E}\cdot\mathbf{D}), \tag{1}$$

where $\mathbf{T}$ and $\mathbf{S}$ are the stress and strain fields, and $\mathbf{E}$ and $\mathbf{D}$ are the electric and electric displacement fields. The piezomechanical interaction can be written in the strain-charge

*hong.tang@yale.edu

form as

$$\mathbf{S} = \mathbf{s}\cdot\mathbf{T} + \mathbf{d}^T\cdot\mathbf{E}, \tag{2}$$

$$\mathbf{D} = \mathbf{d}\cdot\mathbf{T} + \epsilon\cdot\mathbf{E}, \tag{3}$$

where $\mathbf{s}$, ϵ, and $\mathbf{d}$ are the elastic, permittivity, and piezoelectric tensors of the material, respectively. By substituting them into Eq. (1), we obtain the piezoelectric energy,

$$U_{\rm pe} = \frac{1}{2}\int dv(\mathbf{T}\cdot\mathbf{d}^T\cdot\mathbf{E} + \mathbf{E}\cdot\mathbf{d}\cdot\mathbf{T}). \tag{4}$$

The total stress of the mechanical system can be decomposed by the eigenmodes of the unperturbed system as

$$\mathbf{T}(t) = \frac{1}{\sqrt{2}}\sum_m b_m\mathbf{T}^{(m)}e^{-i\Omega_m t} + \text{H.c.}, \tag{5}$$

$$\mathbf{E}(t) = \frac{1}{\sqrt{2}}\sum_n a_n\mathbf{E}^{(n)}e^{-i\omega_n t} + \text{H.c.} \tag{6}$$

Here, b_m and a_n are quantized bosonic operators for the mth mechanical mode and the nth microwave cavity mode, $\mathbf{T}^{(m)}$ and $\mathbf{E}^{(n)}$ are the corresponding normalized field distributions, and Ω_m and ω_n are the eigenmode frequencies.

The Hamiltonian of the piezomechanical system represented by the bosonic operators for phonon $b_m^\dagger$ and microwave photon $a_n^\dagger$ is

$$\mathcal{H}_{\rm pm} = \sum_m \hbar\Omega_m b_m^\dagger b_m + \sum_n \hbar\omega_n a_n^\dagger a_n + \sum_{m,n}\hbar g_{mn}(b_m^\dagger + b_m)(a_n + a_n^\dagger), \tag{7}$$

with coupling strength

$$g_{mn} = \frac{1}{2}\int dv(\mathbf{T}^{(m)}\cdot\mathbf{d}^T\cdot\mathbf{E}^{(n)} + \mathbf{E}^{(n)}\cdot\mathbf{d}\cdot\mathbf{T}^{(m)}). \tag{8}$$

For crystals with hexagon 6 mm (C_{6v}) symmetry, such as AlN and GaN [32], the piezoelectric coefficient tensor has the following form:

$$\mathbf{d}^T = \begin{pmatrix} 0 & 0 & 0 & 0 & d_{15} & 0 \\ 0 & 0 & 0 & d_{24} & 0 & 0 \\ d_{31} & d_{32} & d_{33} & 0 & 0 & 0 \end{pmatrix}, \tag{9}$$

where the first subscript (1,2,3) labels the (x,y,z) components of the vector field $\mathbf{E}$, while the second subscript $(1,2,\ldots,6)$ labels the (xx, yy, zz, yz, xz, xy) components of the tensor field $\mathbf{T}$.

Figure 1(a) shows a simple cavity piezomechanics system, where an inductor-capacitor (LC) circuit serves as a microwave resonator, and a thin aluminum nitride (AlN) film sandwiched by the capacitor is a film bulk acoustic resonator (FBAR). In the capacitor, the displacement field D_3 is constant when the electric fringe effect is neglected. The value of D_3 for a single microwave excitation satisfies $\frac{1}{2}\frac{D_3^2}{\epsilon_0\epsilon_r}A_{\rm C}h + \frac{1}{2}\frac{D_3^2}{\epsilon_0}A_{\rm C}h_s = \frac{1}{2}\hbar\omega_1$. Then we obtain the uniform electric field in the dielectric as

$$E_3^{(1)} = \frac{1}{\epsilon_0\epsilon_{\rm AlN}}\sqrt{\frac{\hbar\omega_1}{A_{\rm C}\left(\frac{h_s}{\epsilon_0} + \frac{h}{\epsilon_0\epsilon_{\rm AlN}}\right)}}. \tag{10}$$

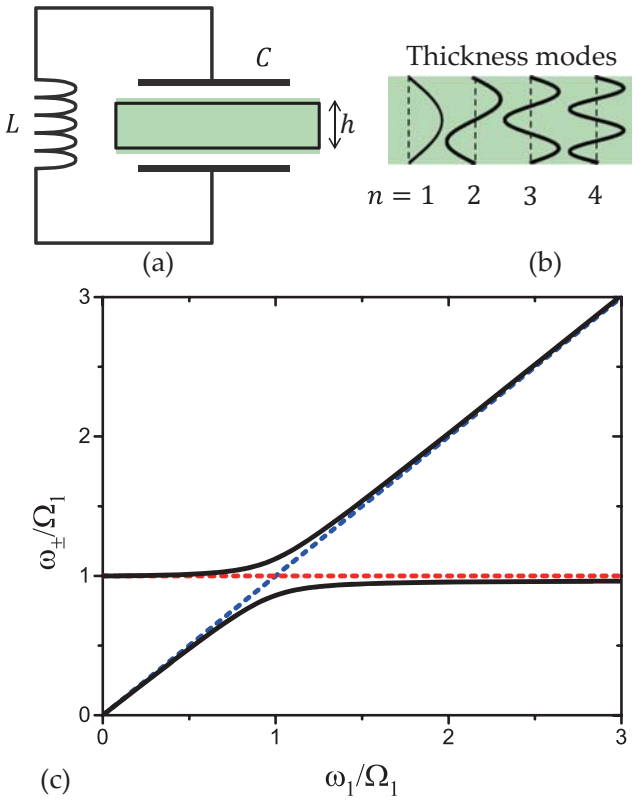

FIG. 1. (a) Schematic illustration of a piezomechanical system. An LC circuit is coupled with a thin aluminum nitride film sandwiched in the capacitor. (b) Distributions of the z-direction strain field of thickness modes (only the first four orders of modes are shown). (c) Normal mode frequencies of the piezomechanical system, in which the AlN film perfectly matches the spacing of the capacitor. ω_1 and Ω_1 are the frequencies of decoupled microwave and fundamental thickness modes, as indicated by the dashed lines.

Here, we have only one mode in the LC circuit at $\omega_1 = 1/\sqrt{LC}$, where L is the inductance and $C = \frac{A_{\rm C}\epsilon_0\epsilon_{\rm AlN}}{h+h_s\epsilon_{\rm AlN}}$ is the capacitance. $A_{\rm C}$ is the area of the capacitor, and h and h_s are the thickness of the AlN and the air spacing in the capacitor, respectively. ϵ_0 is the permittivity of vacuum and $\epsilon_{\rm AlN} = 8.5$ is the relative permittivity of the AlN.

The thickness modes of the thin film satisfy the equation [31] $\frac{\partial^2 u_3}{\partial z^2} = \frac{1}{v_l^2}\frac{\partial^2 u_3}{\partial t^2}$, where u_3 is the displacement in the z direction and v_l is the longitudinal acoustic wave velocity in the material. The solutions have the form $u_3^{(n)}(z,t) = [A\sin(k_n z) + B\cos(k_n z)]e^{-i\Omega_n t}$, with $k_n = \frac{\Omega_n}{v_l}$. Due to the boundary conditions $T_3 = 0$ at $z = 0$ and $z = h$, we have $A\cos(0) - B\sin(0) = 0$, $A\cos(k_n h) - B\sin(k_n h) = 0$. Therefore, $A = 0$, $B = 1$, and $k_n h = n\pi$ for the nth standing acoustic wave modes, as shown in Fig. 1(b). Then, the normalized stress can be solved, $T_3^{(n)} = \sqrt{2\hbar\Omega_n c_{33}/A_{\rm AlN}h}\sin(k_n z)$, by neglecting the effects from the fringe fields, where c_{33} is the elastic constant and $A_{\rm AlN}$ is the area of the AlN film. Substituting the expressions of stress and electric fields into Eq. (8), we obtain the coupling strength,

$$g_{1n} = \xi_n\sqrt{\omega_1\Omega_n}, \tag{11}$$

where the normalized coupling coefficient is

$$\xi_n = \frac{1}{\sqrt{2}} \frac{1-\cos n\pi}{n\pi} \frac{A_{\rm ol}}{\sqrt{A_{\rm C} A_{\rm AlN}}} \times d_{33} \sqrt{\frac{c_{33}}{\epsilon_0 \epsilon_r (\epsilon_r h_s/h+1)}}. \quad (12)$$

Here, $A_{\rm ol} < \min\{A_{\rm AlN}, A_{\rm C}\}$ is the overlapping area between the AlN film and the capacitor.

The hybridization of the fundamental FBAR mode and the LC mode leads to new normal modes whose frequencies are

$$\omega_{\pm}^2 = \frac{\omega_1^2 + \Omega_n^2}{2} \pm \frac{\sqrt{(\omega_1^2 - \Omega_n^2)^2 + 16\xi_n^2 \omega_1 \Omega_n}}{2}. \quad (13)$$

From Eq. (12), the expression $(1-\cos n\pi)/n\pi$ indicates that only odd-order mechanical modes can couple with the LC resonator, and the coupling strength reduces for high-order mechanical modes. The term $A_{\rm ol}/\sqrt{A_{\rm C} A_{\rm AlN}}$ represents the filling factor of the system, which cannot exceed one. Therefore, the largest achievable coupling strength is

$$\xi_1 = \frac{\sqrt{2}}{\pi} d_{33} \sqrt{\frac{c_{33}}{\epsilon_0 \epsilon_{\rm AlN}}}, \quad (14)$$

for $A_{\rm AlN} = A_{\rm C}$ and $h_s = 0$ that correspond to the unity filling factor. Using the experimentally determined material constants of AlN [32–34], $d_{33} = 4.0$ pm/V, $\epsilon_r = 10.4$, $c_{33} = 389$ GPa, $v_l = 11$ km/s, and ξ_1 is estimated to be 0.13. In Fig. 1(c), we plot the frequencies of normal modes for the ideal setup (solid lines), comparing with the uncoupled modes (dashed lines). For $\omega_1 \approx \Omega_1$, the large coupling strength $g_{11} \approx 0.13\Omega_1$ leads to the avoided crossing of modes, with a splitting of about $2g_{11} \approx 0.26\Omega_1$. This value is even comparable with the resonant frequencies of the microwave and the mechanical modes, reaching the so-called ultrastrong-coupling regime [35,36].

III. PIEZOMECHANICS ON AlN CHIPS

Now we propose possible experimental configurations for realizing strong piezomechanical coupling. To be compatible with integrated photonics, we study the piezomechanics on an AlN photonic chip and using the system parameters from Refs. [26,29], where an AlN thin film ($h = 550$ nm) is deposited on a silicon (Si) substrate (thickness is $h_{\rm Si} = 500$ μm), with a 2 μm silicon dioxide (SiO_2) layer between the AlN and the Si. During the fabrication, AlN microstructures, such as waveguides and microcavities, can be suspended by etching away the sacrificial silica layer. The AlN layer, on one hand, confines the visible or telecom photons due to the high refractive index contrast to vacuum; on the other hand, it also supports the mechanical thickness mode to couple to an external 3D microwave cavity or an on-chip microwave resonator.

In the following calculations, we focus on the fundamental thickness mode $n = 1$ with $\Omega/2\pi = v_l/2h = 10$ GHz and assume a mechanical quality factor of $Q_b = 2 \times 10^4$ at low temperatures according to experimental results [26,29]. The corresponding amplitude decay rate of the mechanical mode is $\kappa_b/2\pi \approx 0.25$ MHz. For superconducting microwave cavities, an intrinsic quality factor of $Q_a = 2 \times 10^5$ is feasible [37], which gives $\kappa_{a,0}/2\pi \approx 0.025$ MHz. In the following, we will demonstrate that the strong coupling, in which $g_{\rm pm} > \kappa_b, \kappa_{a,0}$, can be achieved for both 2D and 3D configurations.

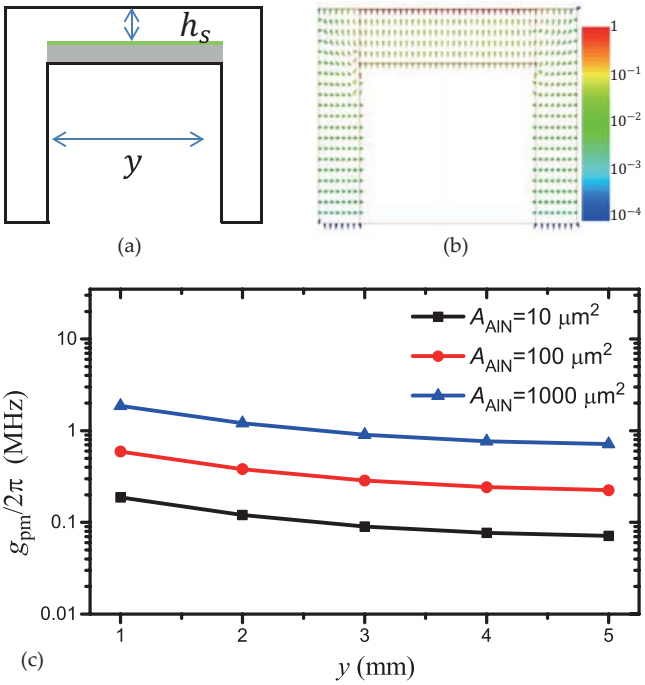

FIG. 2. (a) Schematic illustration of the 3D cavity piezomechanical system configuration. (b) The electric field distribution of the cavity for the square post size $y = 3$ mm. The chip area matches the post with $h_s = 10$ μm and $h_{\rm Si} = 500$ μm. (c) The piezomechanical coupling strength $g_{\rm pm}$ between the fundamental cavity mode and first-order thickness mode for different AlN device areas $A_{\rm AlN} = 10, 100, 1000$ μm^3.

A. 3D cavity

Figure 2(a) shows the schematic of a system, where an AlN-on-Si chip is placed in a 3D microwave cavity. For simplicity, we assume that the AlN microstructure is either waveguide or microring, with width w and length l. To concentrate the electric field to the photonic chip, we adapt a 3D reentrant cavity structure [38,39] that has a square post in the middle. As shown in Fig. 2(b), the electric field is greatly enhanced in the small gap between the post and the top of the cavity.

Based on the numerically simulated electric field distribution, we calculate the piezomechanical coupling strength $g_{\rm pm}$ using Eq. (8). For simplicity, we assume that the electric distribution is not affected by the nonuniform AlN layer and only the Si substrate is included in the numerical model, since the field is mainly determined by the thick Si substrate. By fixing the size of the Si substrate to match the size of the square post and introducing $h_s = 10$-μm-thick spacing between the chip surface and the cavity wall [Fig. 2(a)], we calculate $g_{\rm pm}$ with the simulated electric field on the surface of Si. The results are plotted in Fig. 2(c). Compared with the case without silicon or air spacing, where $g_{\rm pm}/2\pi = 1.3$ GHz, the achievable $g_{\rm pm}$ in the 3D cavity is reduced by more than three orders, due to the additional spacing between the capacitor and the reduced filling factor $F_{\rm 3D} = A_{\rm AlN}/y^2$ for practical devices ($g_{\rm pm} \propto$

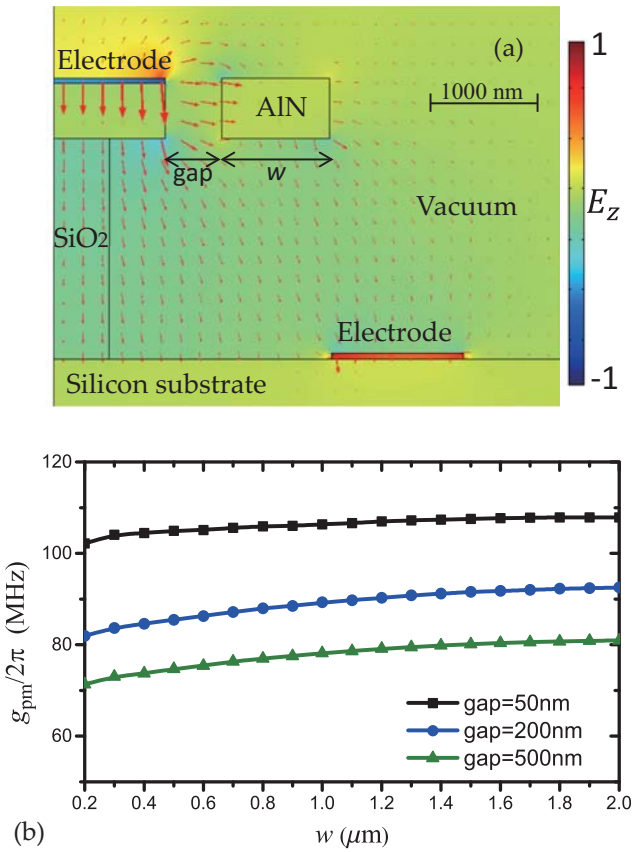

FIG. 3. (a) The cross section of a suspended AlN waveguide coupled with a coplanar microwave resonator, where gap = 500 nm and $w = 1$ μm. The contour plot shows the electric field E_z. The arrows indicate the electric field vectors. (b) The dependence of piezomechanical coupling strength g_{pm} on the waveguide width w for different AlN to electrode gaps.

$\sqrt{A_{AlN}}$ to a given cavity geometry). Considering the dielectric constant of Si substrate $\epsilon_{Si} = 12$ and the spacing $h_s = 10$ μm, we estimate the best achievable coupling strength $g_{pm}/2\pi \approx \frac{\sqrt{2}}{\pi} d_{33}\sqrt{\frac{c_{33}}{\epsilon_0\epsilon_{AlN}}/(\frac{\epsilon_{AlN}h_s}{h} + \frac{\epsilon_{AlN}h_{Si}}{\epsilon_{Si}h} + 1)}\Omega \approx 85$ MHz for $\Omega/2\pi =$ 10 GHz with the A_{AlN} matching the post size ($F_{3D} = 1$). By changing the geometry of the 3D cavity, we find that the g_{pm} decreases monotonously with increasing post size because the cavity mode volume increases with y. For a structure with $w = 1$ μm and $l = 100$ μm, we get $A_{AlN} = 100$ μm^2 and $g_{pm}/2\pi \approx 0.59$ MHz for $y = 1$ mm.

B. Coplanar resonator

Since the 3D microwave cavity has a relatively large mode volume, we also consider the piezomechanics in a planar geometry with integrated superconducting resonators. Figure 3(a) shows a schematic of the proposed structure. To ease the fabrication difficulty, we avoid the implementation of the parallel capacitor which requires a buried electrode below the waveguide. Instead, the bottom electrode is offset from the waveguide to form the ground plane. In addition, to avoid the metal-induced mechanical loss, the top electrode is fabricated beside the waveguide with a gap between them. This arrangement guarantees a considerable portion of the out-of-plane electric field in the waveguide, albeit at a reduced amplitude compared to the parallel plate geometry.

In Fig. 3(a), the electric field distribution for the coplanar microwave resonator by numerical simulation is plotted. Although the AlN is not perfectly sandwiched between electrodes, there is still E_z field in the waveguide where the amplitude is about 20 times smaller than the E_z field in the air beneath the electrode. With the numerically solved electric field distribution, the coupling strength g_{pm} is calculated using Eq. (8), and the results are shown in Fig. 3(b). Here, we set the microwave cavity length to be $\lambda_{mw}/4$, where $\lambda_{mw} \approx 0.03$ m is the wavelength of microwave. Introducing the filling factor $F_{2D} = 4l/\lambda_{mw}$, we have $g_{pm} \propto \sqrt{F_{2D}}$ when $l < \lambda_{mw}/4$. In Fig. 3(b), g_{pm} is calculated with $F_{2D} = 1$. g_{pm} reduces with increasing gap because of the decaying electric field away from the electrode. When the waveguide width w is increased from 0.2 to 2 μm, g_{pm} increases due to larger overlap between the electric field and the AlN structure. As w is further increased, g_{pm} will eventually decrease to zero, as the size of AlN is much larger than the effective volume of microwave fields. For a structure with $w = 1$ μm and $l = 100$ μm, we have $F_{2D} = 0.013$. Then, we have $g_{pm}/2\pi \approx 12.3$ MHz for a 50 nm gap, which is more than two times larger than the results obtained in the 3D case.

IV. PIEZO-OPTOMECHANICS FOR FREQUENCY CONVERSION

Now we study the strong piezomechanical coupling enhanced M-O conversion on the AlN chip. Here, we focus on the optomechanics interaction between the fundamental thickness mechanical mode and the optical mode in photonic microcavities [24,27].

A. The optomechanical coupling

In the optomechanical AlN microstructures, light is confined in the thick AlN film, and the radiation pressure force on the interface expands the film in thickness direction. Reversely, the change of thickness of the film by the mechanical vibration will modify the boundary condition of the electromagnetic field, and thus modulate the optical cavity frequency. Therefore, the optomechanical system can be described by the Hamiltonian

$$H_{om} = \hbar\omega_c c^\dagger c + \hbar\Omega b^\dagger b + \hbar g_{om} c^\dagger c(b^\dagger + b). \quad (15)$$

Here, c denotes the annihilation operator of the optical photon mode. The optical cavity frequency is $\omega_c/2\pi \approx 1.95 \times 10^{14}$ Hz, with the intrinsic material limited loss $\kappa_{c,0}/2\pi =$ 100 MHz for a quality factor of $Q_{c,0} = 10^6$. g_{om} is the vacuum phonon-photon interaction strength and can be estimated as

$$g_{om}^{TE(TM)} \approx \frac{2\omega_c}{n_{eff}^{TE(TM)}} \frac{\partial n_{eff}^{TE(TM)}}{\partial h} u_{zpf} - \frac{2\omega_c}{3h} n^2 p_{13(33)} u_{zpf}, \quad (16)$$

where the first and second terms are due to the photoelastic and moving boundary effects [40–42]. Here, u_{zpf} is the zero-point fluctuation displacement of the film, and $n = 2.2$ and $n_{eff}^{TE(TM)} \approx 1.86(1.73)$ are the refractive index of the AlN and the effect index of the waveguide, respectively.

From numerical simulations of the AlN waveguide, we have $\partial n_{\rm eff}^{\rm TE(TM)}/\partial h = 5.63(13.2)\times 10^{-4}$ nm^{-1} for $h = 550$ nm and $w = 1$ μm. By substituting the $u_{\rm zpf} = \frac{h}{\pi}\sqrt{\frac{2\hbar\Omega}{c_{33}A_{\rm AlN}h}} = 1.02\times 10^{-15}/\sqrt{hwl\times\mu{\rm m}^{-3}}$ m and photoelastic constants of AlN $p_{13(33)} = -0.019(-0.107)$ [43,44] into Eq. (16), we obtain

$$g_{\rm om}^{\rm TE}/2\pi \approx 142.9/\sqrt{hwl\times\mu{\rm m}^{-3}}\ {\rm kHz}, \tag{17}$$

$$g_{\rm om}^{\rm TM}/2\pi \approx 429.2/\sqrt{hwl\times\mu{\rm m}^{-3}}\ {\rm kHz}. \tag{18}$$

Here, the photoelastic effect contributes 15% and 29% for the transverse electric (TE) and transverse magnetic (TM) modes, respectively. According to the experiment results by Bu *et al.* [44], the photoelastic constant might be several times larger than the value we used here, which indicates that the photoelastic effect induced optomechanical coupling is not negligible. Since the $g_{\rm om}^{\rm TM}$ is larger, we just consider the TM optical mode in the following.

B. The piezo-optomechanics

For the purpose of M-O frequency conversion, we need the coherent conversion between b and c. To compensate the energy difference between optical photon and microwave phonons, an external laser driving at frequency $\omega_d \approx \omega_c - \Omega$ is required. As $\Omega \gg \kappa_{a,0},\kappa_b,g_{\rm pm}$, we simply apply the resolved-sideband approximation that neglects the counter-rotating terms, and obtain the effective Hamiltonian

$$H_{\rm eff} = \hbar G_{\rm om}(b^\dagger c + bc^\dagger) + \hbar g_{\rm pm}(ba^\dagger + b^\dagger a), \tag{19}$$

with the effective optical photon-phonon coupling strength $G_{\rm om} = \sqrt{N_d}g_{\rm om}$, where N_d is the intracavity photon number.

The system dynamics incorporating all the interacting modes reads

$$\frac{d}{dt}a = \chi_a a - ig_{\rm pm}b - i\sqrt{2\kappa_{a,1}}A_{\rm in} + \sqrt{2\kappa_a}\tilde{a}, \tag{20}$$

$$\frac{d}{dt}b = \chi_b b - ig_{\rm pm}a - iG_{\rm om}c + \sqrt{2\kappa_b}\tilde{b}, \tag{21}$$

$$\frac{d}{dt}c = \chi_c c - iG_{\rm om}b + \sqrt{2\kappa_c}\tilde{c}, \tag{22}$$

where $\chi_a = -i(\omega_a - \omega_{\rm mw}) - \kappa_a$, $\chi_b = -i(\Omega - \omega_{\rm mw}) - \kappa_b$, $\chi_c = -i(\omega_c - \omega_d - \omega_{\rm mw}) - \kappa_c$, $\kappa_a = \kappa_{a,0} + \kappa_{a,1}$, and $\kappa_c = \kappa_{c,0} + \kappa_{c,1}$. Here, $\kappa_{a,0(1)}$ and $\kappa_{c,0(1)}$ denote the intrinsic (external) loss rate of the microwave and the optical cavity modes. $\tilde{a}$, $\tilde{b}$, and $\tilde{c}$ represent the noise inputs to the system. ω_d is the drive laser frequency and $\omega_{\rm mw}$ is the input microwave frequency. By neglecting the noises, the steady-state conversion efficiency can be solved as

$$T = \frac{2\kappa_{c,1}c^\dagger c}{|A_{\rm in}|^2} = \frac{g_{\rm pm}^2 G_{\rm om}^2 2\kappa_{a,1}2\kappa_{c,1}}{|G_{\rm om}^2\chi_a + g_{\rm pm}^2\chi_c + \chi_a\chi_b\chi_c|^2}. \tag{23}$$

For ideal frequency alignments among input laser and microwave frequencies, we have $\chi_a = -\kappa_a$, $\chi_b = -\kappa_b$, and $\chi_c = -\kappa_c$; then,

$$T = \frac{\kappa_{a,1}}{\kappa_a}\frac{\kappa_{c,1}}{\kappa_c}\frac{4\frac{g_{\rm pm}^2}{\kappa_b\kappa_a}\frac{G_{\rm om}^2}{\kappa_b\kappa_c}}{\left[\frac{G_{\rm om}^2}{\kappa_b\kappa_c} + \frac{g_{\rm pm}^2}{\kappa_b\kappa_a} + 1\right]^2}. \tag{24}$$

C. Conversion efficiency

Although $G_{\rm om}$ can be enhanced by the parametric laser drive, the ultimate achievable coupling strength is limited by the material's power handling. For instance, as a rule of thumb, the maximum power delivered to the waveguide without damaging the waveguide is of the order of $P_{\rm crit} = 1$ W/μm^2. In the cavity, the equivalent circulating power is

$$P = \frac{N_d\hbar\omega_d/(l/v_g)}{hw} = \frac{N_d\hbar\omega_d v_g}{hwl}, \tag{25}$$

where v_g is the group velocity of light. The power handling of the material requires $P < P_{\rm crit}$, corresponding to $N_d/hwl \leqslant 5\times 10^4$ μm^{-3}, giving rise to the maximum achievable linear optomechanical coupling strength,

$$G_{\rm om}/2\pi \leqslant 96.0\ {\rm MHz}. \tag{26}$$

Note that this maximum value is independent of the size of the AlN photonic structure, regardless of the value of the $g_{\rm pm}$, which can be adjusted by changing the filling factor of the microstructures.

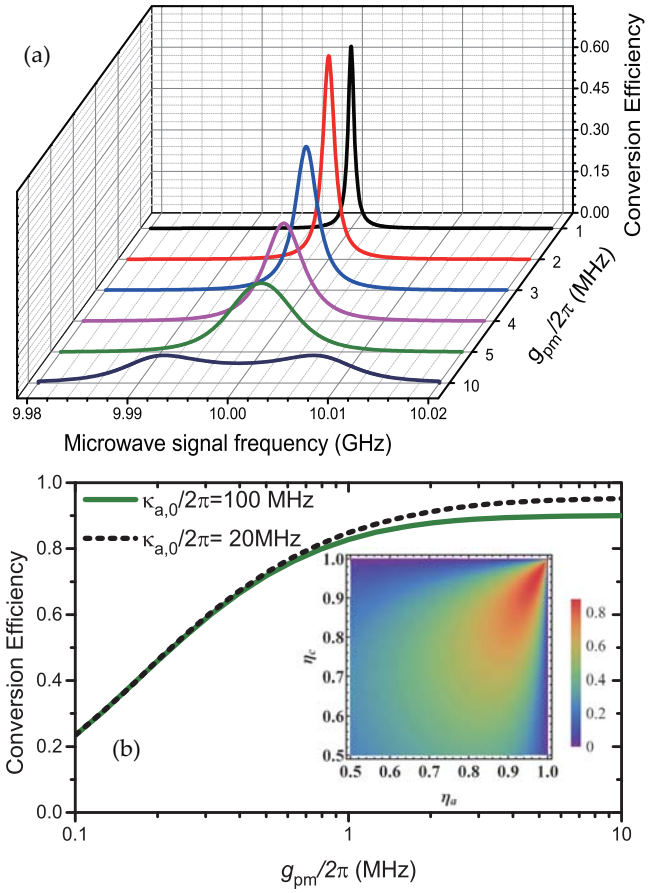

FIG. 4. (a) The frequency dependence of the conversion efficiency ξ for different $g_{\rm pm}/2\pi = 1,2,3,4,5,10$ MHz. (b) The optimal conversion efficiency for a given $g_{\rm pm}$, by optimizing cavity extraction ratios η_a and η_c. The solid (dashed) lines correspond to intrinsic optical dissipation rates $\kappa_{c,0}/2\pi = 100\,(20)$ MHz. The inset shows the conversion efficiency against η_a and η_c, with $g_{\rm pm}/2\pi = 2$ MHz. Other parameters: $g_{\rm om}/2\pi = 96.0$ MHz, $\omega_a = \omega_b$, $\omega_d = \omega_c - \omega_b$, $\{\kappa_{c,0},\kappa_b,\kappa_{a,0}\}/2\pi = \{100,0.25,0.025\}$ MHz.

According to Eq. (24), large $G_{\rm om}$ and $g_{\rm pm}$ are preferred for efficient internal frequency conversion. The optimal condition requires $\frac{g_{\rm pm}^2}{\kappa_b\kappa_a} \approx \frac{G_{\rm om}^2}{\kappa_b\kappa_c} \gg 1$, which means that $g_{\rm pm}$ should be optimized according to the $G_{\rm om}$, κ_a, and κ_c. In addition, the other two parameters—the extraction ratio $\eta_a = \frac{\kappa_{a,1}}{\kappa_{a,0}+\kappa_{a,1}}$ and the input coupling ratio $\eta_c = \frac{\kappa_{c,1}}{\kappa_{c,0}+\kappa_{c,1}}$—should be optimized for achieving high output efficiency. Here, the intrinsic loss rates ($\kappa_{a,0}$ and $\kappa_{c,0}$) are constant, while external coupling rates ($\kappa_{a,1}$ and $\kappa_{c,1}$) are adjustable by varying the structure geometry.

Figure 4(a) shows the microwave signal conversion efficiency against the input signal frequency for various piezomechanical coupling strength $g_{\rm pm}$, with fixed $\eta_a = \eta_c = 0.9$. At increased $g_{\rm pm}$, the bandwidth of the conversion increases, while the best efficiency is obtained for optimal $g_{\rm pm}$. From the spectrum for $g_{\rm pm}/2\pi = 10$ MHz, we can see two peaks due to the strong coupling. These results indicate that for different $g_{\rm pm}$, we should choose optimal η_a and η_c for best conversion efficiency. The inset of Fig. 4(b) plots the conversion efficiency as a function of η_a and η_c with fixed $g_{\rm pm}/2\pi = 2$ MHz. It can be seen that the optimal conversion efficiency $T = 0.877$ is realized at $\eta_a = 0.977$, $\eta_c = 0.961$.

Therefore, we numerically solve the optimal conversion efficiency T for on-resonance microwave signal and different $g_{\rm pm}$. The result is shown as a solid curve in Fig. 4(b); the conversion efficiency monotonously increases with $g_{\rm pm}$ and saturates to $T \approx 0.9$ when $g_{\rm pm}/2\pi > 3$ MHz. By introducing the intrinsic cooperativities $C_{\rm om} = \frac{G_{\rm om}^2}{\kappa_b\kappa_{c,0}}$ and $C_{\rm pm} = \frac{g_{\rm pm}^2}{\kappa_b\kappa_{a,0}}$, we can asymptotically solve the optimal condition for Eq. (24) as $\kappa_{a,1} \approx \kappa_{a,0}C_{\rm pm}/\sqrt{C_{\rm om}}$ and $\kappa_{c,1} \approx \kappa_{c,0}\sqrt{C_{\rm om}}$ for $C_{\rm pm} \gg C_{\rm om} \gg 1$. In this case, the optimal achievable conversion efficiency is

$$T_{\rm sat} \approx \frac{C_{\rm om}}{\left(\sqrt{C_{\rm om}+1}+1\right)^2} \approx 1 - \frac{1}{\sqrt{C_{\rm om}}} + O\left(\frac{1}{C_{\rm om}}\right), \quad (27)$$

which is insensitive to the $g_{\rm pm}$. Therefore, the efficiency is saturated due to the intrinsic optical quality factor limited $C_{\rm om} \sim 400$, leading to $T_{\rm sat} \approx 0.9$. If we increase the intrinsic optical quality factor by five times, i.e., $\kappa_{c,0}/2\pi = 20$ MHz, the saturated efficiency can be increased to $T_{\rm sat} \approx 0.95$, which agrees with the numerical results [dashed line in Fig. 4(b)].

With reasonable parameters $g_{\rm pm}/2\pi = 5$ MHz, the optimum conversion can be obtained with $\eta_a = 0.995$ and $\eta_c = 0.95$. The effective frequency conversion efficiency is 0.896, with a bandwidth about 5.6 MHz. If the ambient temperature is 2 K, the corresponding thermal excitation at 10 GHz is $n_{\rm th} = 3.6$, and the added noise during the microwave to optical frequency conversion is $n_{\rm add} \approx 0.22$ [19].

V. CONCLUSION

In conclusion, the piezomechanical strong coupling is proposed and investigated using practical device parameters. The numerical simulations show that strong coupling can be achieved for microstructures in an AlN chip coupled to microwave cavity photons in both three-dimensional microwave cavities and planar superconducting resonators. Leveraging the piezomechanical strong coupling will lead to greatly enhanced microwave to optical frequency conversion. With practical parameters, we show that the optimal conversion efficiency can approach 90%, with a bandwidth exceeding 5 MHz and added noise below 0.22. Compared to other electromechanical schemes, the piezo-optomechanical system has several advantages and is very promising for experiments. Thus, piezomechanics in a photonic chip is a promising platform for building future hybrid quantum technologies and integrated photonics.

ACKNOWLEDGMENTS

We thank L. Fan for discussions. We acknowledge the support from Laboratory of Physical Sciences (LPS), Air Force Office of Scientific Research (AFOSR) MURI program, and DARPA ORCHID program. L.J. was also supported by the ARL-CDQI, Army Research Office (ARO), Alfred P. Sloan Foundation, and Packard Foundation.

[1] C. A. Regal and K. W. Lehnert, From cavity electromechanics to cavity optomechanics, J. Phys. Conf. Ser. **264**, 012025 (2011).
[2] S. Barzanjeh, M. Abdi, G. J. Milburn, P. Tombesi, and D. Vitali, Reversible Optical-to-Microwave Quantum Interface, Phys. Rev. Lett. **109**, 130503 (2012).
[3] M. A. Sillanpää and P. J. Hakonen, Optomechanics: Hardware for a quantum network, Nature (London) **507**, 45 (2014).
[4] L. Tian, Optoelectromechanical transducer: Reversible conversion between microwave and optical photons, Ann. Phys. **527**, 1 (2015).
[5] G. Kurizki, P. Bertet, Y. Kubo, K. Mølmer, D. Petrosyan, P. Rabl, and J. Schmiedmayer, Quantum technologies with hybrid systems, Proc. Natl. Acad. Sci. **112**, 3866 (2015).
[6] H. J. Kimble, The quantum internet, Nature (London) **453**, 1023 (2008).
[7] S. Muralidharan, L. Li, J. Kim, N. Lütkenhaus, M. D. Lukin, and L. Jiang, Optimal architectures for long distance quantum communication, Sci. Rep. **6**, 20463 (2016).
[8] Z.-Q. Yin, W. L. Yang, L. Sun, and L. M. Duan, Quantum network of superconducting qubits through an optomechanical interface, Phys. Rev. A **91**, 012333 (2015).
[9] S. Huang, Quantum state transfer in cavity electro-optic modulators, Phys. Rev. A **92**, 043845 (2015).
[10] M. Abdi, P. Tombesi, and D. Vitali, Entangling two distant noninteracting microwave modes, Ann. Phys. **527**, 139 (2015).
[11] K. Zhang, F. Bariani, Y. Dong, W. Zhang, and P. Meystre, Proposal for an Optomechanical Microwave Sensor at the Subphoton Level, Phys. Rev. Lett. **114**, 113601 (2015).
[12] S. Barzanjeh, M. C. de Oliveira, and S. Pirandola, Microwave photodetection with electro-opto-mechanical systems, arXiv:1410.4024.
[13] S. Barzanjeh, S. Guha, C. Weedbrook, D. Vitali, J. H. Shapiro, and S. Pirandola, Microwave Quantum Illumination, Phys. Rev. Lett. **114**, 080503 (2015).
[14] M. Tsang, Cavity quantum electro-optics, Phys. Rev. A **81**, 063837 (2010).

[15] M. Tsang, Cavity quantum electro-optics. II. Input-output relations between traveling optical and microwave fields, Phys. Rev. A **84**, 043845 (2011).

[16] C. Javerzac-Galy, K. Plekhanov, N. Bernier, L. D. Toth, A. K. Feofanov, and T. J. Kippenberg, On-chip microwave-to-optical quantum coherent converter based on a superconducting resonator coupled to an electro-optic microresonator, arXiv:1512.06442.

[17] L. A. Williamson, Y.-H. Chen, and J. J. Longdell, Magneto-Optic Modulator with Unit Quantum Efficiency, Phys. Rev. Lett. **113**, 203601 (2014).

[18] S. A. McGee, D. Meiser, C. A. Regal, K. W. Lehnert, and M. J. Holland, Mechanical resonators for storage and transfer of electrical and optical quantum states, Phys. Rev. A **87**, 053818 (2013).

[19] R. W. Andrews, R. W. Peterson, T. P. Purdy, K. Cicak, R. W. Simmonds, C. A. Regal, and K. W. Lehnert, Bidirectional and efficient conversion between microwave and optical light, Nat. Phys. **10**, 321 (2014).

[20] A. Pitanti, J. M. Fink, A. H. Safavi-Naeini, J. T. Hill, C. U. Lei, A. Tredicucci, and O. Painter, Strong opto-electro-mechanical coupling in a silicon photonic crystal cavity, Opt. Express **23**, 3196 (2015).

[21] X. Zhang, N. Zhu, C.-L. Zou, and H. X. Tang, Optomagnonic whispering gallery microresonators, arXiv:1510.03545.

[22] A. Osada, R. Hisatomi, A. Noguchi, Y. Tabuchi, R. Yamazaki, K. Usami, M. Sadgrove, R. Yalla, M. Nomura, and Y. Nakamura, Cavity Optomagnonics with Spin-Orbit Coupled Photons, Phys. Rev. Lett. **116**, 223601 (2016).

[23] A. D. O'Connell, M. Hofheinz, M. Ansmann, R. C. Bialczak, M. Lenander, E. Lucero, M. Neeley, D. Sank, H. Wang, M. Weides, J. Wenner, J. M. Martinis, and A. N. Cleland, Quantum ground state and single-phonon control of a mechanical resonator, Nature (London) **464**, 697 (2010).

[24] J. Bochmann, A. Vainsencher, D. D. Awschalom, and A. N. Cleland, Nanomechanical coupling between microwave and optical photons, Nat. Phys. **9**, 712 (2013).

[25] L. Fan, X. Sun, C. Xiong, C. Schuck, and H. X. Tang, Aluminum nitride piezo-acousto-photonic crystal nanocavity with high quality factors, Appl. Phys. Lett. **102**, 153507 (2013).

[26] K. Y. Fong, L. Fan, L. Jiang, X. Han, and H. X. Tang, Microwave-assisted coherent and nonlinear control in cavity piezo-optomechanical systems, Phys. Rev. A **90**, 051801 (2014).

[27] L. Fan, K. Y. Fong, M. Poot, and H. X. Tang, Cascaded optical transparency in multimode-cavity optomechanical systems, Nat. Commun. **6**, 5850 (2015).

[28] K. C. Balram, M. Davanco, J. D. Song, and K. Srinivasan, Coherent coupling between radio frequency, optical, and acoustic waves in piezo-optomechanical circuits, Nat. Photon. **10**, 346 (2016).

[29] X. Han, K. Y. Fong, and H. X. Tang, A 10-GHz film-thickness-mode cavity optomechanical resonator, Appl. Phys. Lett. **106**, 161108 (2015).

[30] J. Yang, *An Introduction to the Theory of Piezoelectricity*, Vol. 9 (Springer Science & Business Media, New York, 2005).

[31] K.-y. Hashimoto, *RF Bulk Acoustic Wave Filters for Communications* (Artech House, Norwood, MA, 2009).

[32] I. L. Guy, S. Muensit, and E. M. Goldys, Extensional piezoelectric coefficients of gallium nitride and aluminum nitride, Appl. Phys. Lett. **75**, 4133 (1999).

[33] D. Gerlich, S. Dole, and G. Slack, Elastic properties of aluminum nitride, J. Phys. Chem. Solids **47**, 437 (1986).

[34] M.-A. Dubois and P. Muralt, Properties of aluminum nitride thin films for piezoelectric transducers and microwave filter applications, Appl. Phys. Lett. **74**, 3032 (1999).

[35] T. Niemczyk, F. Deppe, H. Huebl, E. P. Menzel, F. Hocke, M. J. Schwarz, J. J. Garcia-Ripoll, D. Zueco, T. Hümmer, E. Solano, A. Marx, and R. Gross, Circuit quantum electrodynamics in the ultrastrong-coupling regime, Nat. Phys. **6**, 772 (2010).

[36] X. Zhang, C.-l. Zou, L. Jiang, and H. X. Tang, Strongly Coupled Magnons and Cavity Microwave Photons, Phys. Rev. Lett. **113**, 156401 (2014).

[37] A. Megrant, C. Neill, R. Barends, B. Chiaro, Y. Chen, L. Feigl, J. Kelly, E. Lucero, M. Mariantoni, P. J. J. O'Malley, D. Sank, A. Vainsencher, J. Wenner, T. C. White, Y. Yin, J. Zhao, C. J. Palmstrøm, J. M. Martinis, and A. N. Cleland, Planar superconducting resonators with internal quality factors above one million, Appl. Phys. Lett. **100**, 113510 (2012).

[38] N. C. Carvalho, Y. Fan, J.-M. Le Floch, and M. E. Tobar, Piezoelectric voltage coupled reentrant cavity resonator, Rev. Sci. Instrum. **85**, 104705 (2014).

[39] M. Goryachev and M. E. Tobar, The 3D split-ring cavity lattice: A new metastructure for engineering arrays of coupled microwave harmonic oscillators, New J. Phys. **17**, 023003 (2015).

[40] J. Chan, A. H. Safavi-Naeini, J. T. Hill, S. Meenehan, and O. Painter, Optimized optomechanical crystal cavity with acoustic radiation shield, Appl. Phys. Lett. **101**, 081115 (2012).

[41] C. Baker, W. Hease, D.-T. Nguyen, A. Andronico, S. Ducci, G. Leo, and I. Favero, Photoelastic coupling in gallium arsenide optomechanical disk resonators, Opt. Express **22**, 14072 (2014).

[42] K. C. Balram, M. Davanço, J. Y. Lim, J. D. Song, and K. Srinivasan, Moving boundary and photoelastic coupling in GaAs optomechanical resonators, Optica **1**, 414 (2014).

[43] S. Y. Davydov, Evaluation of physical parameters for the group III nitrates: BN, AlN, GaN, and InN, Semiconductors **36**, 41 (2002).

[44] G. Bu, M. S. Shur, D. Ciplys, R. Rimeika, R. Gaska, and Q. Fareed, Guided-wave acousto-optic diffraction in $Al_xGa_{1-x}N$ epitaxial layers, Appl. Phys. Lett. **85**, 2157 (2004).